Research Paper

# Tracking Perfluorocarbon Nanoemulsion Delivery by ^{19}F MRI for Precise High Intensity Focused Ultrasound Tumor Ablation

Soo Hyun Shin[1], Eun-Joo Park[2✉], Changki Min[1], Sun Il Choi[1], Soyeon Jeon[1], Yun-Hee Kim[1], Daehong Kim[1✉]

1. Molecular Imaging & Therapy Branch, Division of Precision Medicine, National Cancer Center, Goyang, Korea;
2. Dept. of Radiology, Seoul National University Hospital, Seoul, Korea

✉ Corresponding author: Daehong Kim, Ph.D. National Cancer Center, Molecular Imaging & Therapy Branch, Division of Precision Medicine, Research Bldg., Ilsanro-323, Ilsandong-gu, Goyang, Korea, 10408; Phone: +82-31-920-2513; E-mail: dkim@ncc.re.kr. Eun-Joo Park, Ph.D. Seoul National University Hospital, Dept. of Radiology, 101 Daehak-ro, Jongno-gu, Seoul, Korea, 03080; Phone: +82-2-2072-4358; E-mail: ejpark@snuh.org.

## Abstract

Perfluorocarbon nanoemulsions (PFCNEs) have recently been undergoing rigorous study to investigate their ability to improve the therapeutic efficacy of tumor ablation by high intensity focused ultrasound (HIFU). For precise control of PFCNE delivery and thermal ablation, their accumulation and distribution in a tumor should be quantitatively analyzed. Here, we used fluorine-19 (^{19}F) magnetic resonance imaging (MRI) to quantitatively track PFCNE accumulation in a tumor, and analyzed how intra-tumoral PFCNE quantities affect the therapeutic efficacy of HIFU treatment. Ablation outcomes were assessed by intra-voxel incoherent motion analysis and bioluminescent imaging up to 14 days after the procedure. Assessment of PFCNE delivery and treatment outcomes showed that 2–3 mg/mL of PFCNE in a tumor produces the largest ablation volume under the same HIFU insonation conditions. Histology showed varying degrees of necrosis depending on the amount of PFCNE delivered. [19]F MRI promises to be a valuable platform for precisely guiding PFCNE-enhanced HIFU ablation of tumors.

Key words: Perfluorocarbon nanoemulsion (PFCNE), ^{19}F MRI, High Intensity Focused Ultrasound (HIFU), Tumor Ablation, Diffusion MR

## Introduction

High intensity focused ultrasound (HIFU) is a promising non-invasive therapy that thermally and/or mechanically ablates tumors. This procedure has been approved by the United States Food and Drug Administration for the treatment of uterine fibroids, prostate cancer and for palliative care in bone metastasis patients [1]. Preclinical and clinical studies for treating other types of tumors including breast, brain, and liver are also underway [2-5]. Because of the long treatment time, microbubbles (MBs) are being investigated for their potential to reduce the acoustic energy and treatment time required for ablation of tumors. However, MBs have a short half-life in the bloodstream (an order of minutes), and their micron-scale sizes preclude their extravasation and accumulation in the tumor interstitium through the enhanced permeation and retention (EPR) effect.

Nano-sized droplets and emulsions composed of perfluorocarbon (PFC) molecules have been highlighted as an alternative of MBs [6-8]. Upon HIFU insonation, PFC nanoemulsions (PFCNE) rapidly vaporize to MBs through a process called acoustic droplet vaporization and initiate cavitation activity. These PFCNEs show significantly longer circulation time and are smaller in size (~200 nm), making them suitable for improved extravasation through the leaky

vasculature of a tumor. Owing to such advantages, PFCNEs are also currently being assessed as ultrasound-triggered drug carriers that can synergistically treat tumors in conjunction with HIFU [9-11].

Considering the heterogeneous nature of a tumor microenvironment, the amount of PFCNEs delivered to a tumor can be highly variable even if delivery parameters, such as nanoemulsion formulation, injection dosage, and delivery route, remain constant [12]. For efficient and reproducible HIFU treatment, the delivery of PFCNEs to a tumor should be visualized in a quantitative fashion so that their amount and distribution can be correlated with the treatment outcome. With this information, PFCNE formulation and HIFU conditions can be optimized for each tumor, leading to precise, safe and rapid ablation of tumors.

Currently, HIFU treatment is usually guided by either ultrasonography (US) or magnetic resonance imaging (MRI) to monitor the treatment procedure and outcome. US directly detects the cavitation activity of PFCNE upon HIFU insonation on a real-time basis; however, the quantification of PFCNE load and distribution in a tumor is difficult. In case of MRI, MBs and PFCNEs can be visualized by incorporating contrast agents such as iron oxide or manganese oxide-based nanoparticles [13-15]. Once these nanoparticles are involved, however, multi-parametric analyses including thermometry cannot be performed as nearby proton spins are perturbed, losing the primary advantage of MR-guided HIFU.

We hypothesized that introducing fluorine-19 ($^{19}$F) MRI during HIFU treatment would enhance the quality of such treatment by non-invasively quantifying PFCNE delivery to tumors without interfering with MR-based parametric analyses of treatment procedures and outcomes. Aside from its role as a precursor of MBs, PFCNE has been widely used as a tracer agent of $^{19}$F MRI, especially for tracking cellular therapeutics and host macrophages in inflammatory disease models [16-19]. The lack of fluorine atoms in biological tissues allows unambiguous detection of signals from PFCNEs as 'hot spots' [20]. As $^{19}$F MRI directly detects fluorine atoms, the relationship between the amount of fluorine and corresponding MR signal intensity is linear, enabling facile signal quantification.

In this study, we used $^{19}$F MRI to monitor the accumulation of PFCNE in a mouse tumor model. Different PFCNE dosages were administered to mice through intravenous injection to achieve a wide range of PFCNE concentrations in tumors, followed by HIFU treatment with the same acoustic conditions.

Intra-voxel incoherent motion (IVIM) analysis and bioluminescence imaging (BLI) were performed to assess the therapeutic efficacy of HIFU treatment, which were confirmed by histology.

## Materials & Methods

### PFCNE Formulation and Characterization

PFCNEs were formulated using a previous protocol with a subtle modification [21, 22]. In brief, 60 mg/mL of Lutrol F68 (BASF, Ludwigshafen, Germany), 4 μL/mL 1,1'-dioctadecyl-3,3,3',3'-tetramethylindocarbocyanine perchlorate (DiI; Molecular Probes, Eugene, OR, USA) and 60% w/v perfluoro-15-crown-5-ether (PCE; Matrix Scientific, Columbia, SC, USA) were mixed in phosphate buffered saline (PBS; Gibco, Waltham, MA, USA). The mixture was emulsified by sonication for 10 minutes in ice-cold water in pulsed mode (2 s on/2 s off) at 1.5 W power using a Sonicator 3000 (Misonix, Farmingdale, NY, USA). The resulting emulsions were filter-sterilized (0.2 μm; Sartorius Stedim, Aubagne, France) and kept at 4 $^\circ$C until use. The size and polydispersity index (PDI) of the PFCNEs were measured by dynamic light scattering (Malvern Zetasizer, Worcestershire, UK), and cytotoxicity was measured using a trypan blue exclusion assay in HCT116 human colon cancer cells. PFCNE morphologies were observed via transmission electron microscopy at an accelerating voltage of 120 kV (JEM-2010; JEOL Ltd., Tokyo, Japan).

### Ex Vivo Simulation of HIFU

For *ex vivo* simulation of HIFU treatment, egg white-based phantoms were prepared [23]. Briefly, 35% v/v egg white, 31.4% v/v degassed deionized water, 33% acrylamide-bisacrylamide (Sigma Aldrich, St. Louis, MO, USA), 0.5% v/v ammonium persulfate (Sigma Aldrich), 0.1% v/v tetramethylethylenediamine (TEMED, Sigma Aldrich), and either 0.1, 0.5, or 1% v/v of PFCNE were mixed, degassed, and cross-linked. The resulting phantom was insonated with HIFU (f = 1.05 MHz) in a continuous mode for 15 s at peak-negative pressures of 2.51 MPa, 3.01 MPa, 3.52 MPa, or 4.27 MPa. The volumes of the resulting lesions were optically measured using the following formula: volume = $w^2 h \pi / 6$, where $h$ and $w$ refer to the height and width of a lesion, respectively.

### Animal Preparation

All animal experiments were performed under Institutional Animal Care and Use Committee (IACUC; Approval number: NCC-15-249) guidelines provided by the National Cancer Center, Korea. For a subcutaneous tumor model, HCT116 cells expressing luciferase were cultured in RPMI-1640 media

(HyClone, Logan, UT, USA) supplemented with 10% fetal bovine serum (Cellgro, Tewksbury, MA, USA) and 1% antibiotics (Gibco, Grand Island, NY, USA) at $37\,^{\circ}$C in a 5% $CO_2$ incubator. Six-week old female BALB/c-nu mice were subcutaneously injected into the left flank with $5 \times 10^6$ cells suspended in 100 µL of 5 mg/mL Matrigel (Corning, Corning, NY, USA) in PBS. Tumors were grown for 2 weeks until attaining a volume of 150–200 mm$^3$ before HIFU treatment.

### In vivo Study Design

Forty-eight hours before the first MRI and BLI, mice were intravenously injected with 50 µL (n = 5; PFC50+), 100 µL (n = 4; PFC100+), or 200 µL (n = 4; PFC200+) of PFCNE through their tail veins. The 48-hour time point was chosen upon considering the blood half-life of similar PFCNEs in previous studies, and allowed for maximum accumulation in tumors [24, 25]. For the group receiving 400 µL of PFCNE (n = 6; PFC400+), the injection was administered over 2 days (48 and 24 hours before the first MR scan) using 200 µL per day to allow mice to adapt to increased circulation volume. Untreated mice (n = 5; control) and a group treated without PFCNE (n = 5; PFC-) were also included. MRI and BLI were performed up to 2 weeks following the HIFU insonation. A schematic illustration describing the *in vivo* experimental procedure is shown in Fig. 1.

### In vivo MRI

MR images were acquired using a 7T scanner (BioSpec 70/20 USR; Bruker, Billerica, MA, USA) and a custom-made $^1$H/$^{19}$F-double tune 35 mm volume coil. Mice were anesthetized with 2% isoflurane gas, and their respiration rates were monitored during the scans. For proton anatomical images, rapid acquisition with relaxation enhancement (RARE) sequence was used with the following parameters: repetition time (TR)/echo time (TE) = 2600/30 ms, number of average (NA) = 2, RARE factor = 4, matrix = 256 × 192, slice thickness (ST) = 1.25 mm, and field of view = 4 × 3 cm. Diffusion-weighted images (DWIs) and $^{19}$F images were also acquired (DWI: Spin Echo, TR/TE = 2000 / 26 ms, matrix = 192 × 128, b-values = 0, 45, 350, 1000, and 2000 s/mm$^2$; $^{19}$F: FLASH, TR/TE = 50/2.5 ms, matrix = 64 × 48, NA = 512, receive bandwidth = 25 kHz, echo position = 30%, ST = 2.5 mm). For $^{19}$F imaging, a reference tube with 5 mg/mL of PFCNE in acrylamide gel was placed adjacent to a mouse for signal quantification purpose. Before signal quantification, raw $^{19}$F images were corrected for Rician noise distribution as previously described [26]. The processed images were rendered in a pseudo-color scale and superimposed on corresponding proton images.
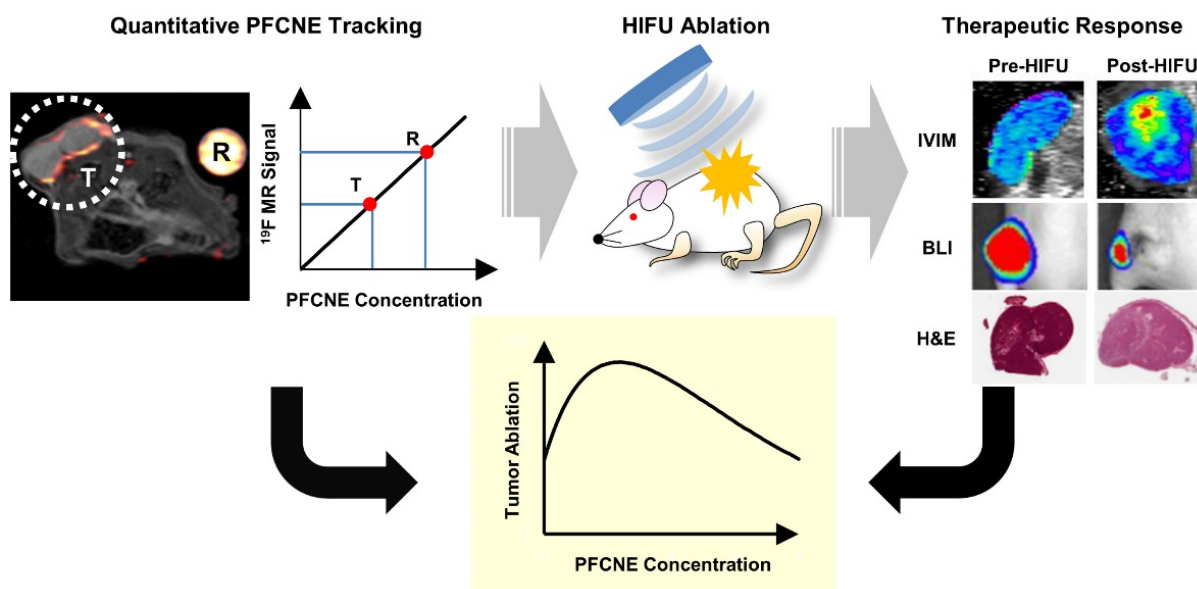


**Figure 1.** Schematic illustration showing the usage of $^{19}$F MRI for efficient and reproducible perfluorocarbon nanoemulsion (PFCNE)-enhanced high intensity focused ultrasound (HIFU) tumor ablation. Owing to the heterogeneous tumor microenvironment, the accumulation of PFCNE in a tumor can be highly variable, leading to unpredictable therapeutic outcomes after HIFU treatment. Using $^{19}$F MRI, the concentration of PFCNE in a tumor can be quantified via imaging along by using a reference containing a known concentration of PFCNE. HIFU treatment can be performed after the quantification process, followed by evaluation of therapeutic outcomes. Afterwards, the PFCNE concentration in a tumor, as measured by $^{19}$F MRI, can be correlated with therapeutic outcomes. This information will enable the prediction of the therapeutic outcomes at given concentrations of PFCNE, as well as the optimization of the parameters involved in PFCNE accumulation in a tumor (such as PFCNE formulation and delivery route) for efficient HIFU tumor ablation.

## IVIM Analysis

IVIM maps were generated by nonlinear least squares fitting of DWIs with the 5 different b-values indicated above in the following bi-exponential model [27, 28]:

$$S_b/S_0 = (1-\mathrm{f})e^{-bD_t} + fe^{-bD_p}$$

in which $S_0$ = signal intensity at the b-value of 0; $S_b$ = signal intensity at a given b-value other than 0; f = microvascular volume fraction; $D_t$ = true diffusion coefficient of water molecule; and $D_p$ = pseudo-diffusion coefficient due to microcirculation. A custom-written program based on Interactive Data Language (IDL 8.2.2; Exelis Visual Information Solutions, Inc., Boulder, CO, USA) was used for the fitting process. The region of interest (ROI) was manually drawn over a tumor, and pixels with $D_t$ values higher than 150% of the median of untreated tumors ($7.5 \times 10^{-4}$ mm$^2$/s) were analyzed for delineation of lesions formed by HIFU ablation.

## BLI

Mice were anesthetized with 2% isoflurane gas during imaging; 150 mg/kg body weight of D-luciferin (Gold Biotechnology Inc., St. Louis, MO, USA) was injected into the peritoneal cavities of mice and imaged 20 minutes after the injection using a Xenogen IVIS Spectrum (Perkin Elmer, Waltham, MA, USA). Acquired images were processed with Living Image 2.6 software (Perkin Elmer). ROIs with the same area were placed on tumors for signal measurement.

## Ex Vivo Fluorescence Imaging

Three additional mice from each group injected with PFCNE were sacrificed without HIFU treatment after confirming the accumulation of PFCNE in tumors via $^{19}$F MRI. Tumors were excised and imaged using the Xenogen IVIS Spectrum system with a DsRed filter (excitation passband: 500–550 nm; emission passband: 575–650 nm). Acquired images were processed with Living Image 2.6 software, and the signals from the tumors were quantified.

## HIFU Treatment

Each mouse was placed on a degassed water bath beneath which a single-element transducer (diameter: 4 cm, focal distance: 3.5 cm) was positioned. Mice were subjected to a single-shot HIFU (f = 1.05 MHz) for 15 s in a continuous mode at the peak-negative pressure of 3.52 MPa. The focal size (-3 dB) was 0.87 mm in diameter and 5.4 mm in length.

## Histological Analysis

Immediately after HIFU treatment, 3 additional mice from each HIFU-treated group were sacrificed. Tumors were excised and fixed in 4% paraformaldehyde for 24 hours. Fixed tumors were embedded in paraffin blocks, and 4-μm thick sections were made for hematoxylin and eosin (H&E) staining. H&E-stained sections were imaged with Aperio Scan Scope XT (Leica Biosystems, Heidelberg, Germany) at 200× magnification.

## Statistical Analysis

All statistical analyses were performed using GraphPad Prism 5 (GraphPad Software, La Jolla, CA, USA) and Microsoft Excel 2010 (Microsoft, Seattle, WA, USA). For multi-group comparisons, one-way ANOVA was performed followed by Bonferroni correction. Pearson's test was performed for correlation analyses. Two-tailed p-values less than 0.05 were considered statistically significant. All data values are represented as the mean ± standard error of the mean unless otherwise indicated.

## Results

### Characterization of PFCNEs

The average PFCNE diameter was 159 ± 2.7 nm and PDI was 0.08 ± 0.02 after production (Fig. 2D). The size and dispersity of PFCNEs remained stable at 4 °C for up to 3 weeks, while sizes increased with time at 25 °C and 37 °C (Fig. 2E). Stability was not significantly affected by serum (Fig. 2F). The viability of HCT116 cells was not affected by PFCNEs in the culture media at increasing concentrations up to 30 mg/mL (Fig. 2G). To validate the $^{19}$F MR signal quantification, a fluorescent dye was incorporated into PFCNEs. MR and fluorescence images of PFCNE-incorporated phantoms were acquired, and signals from these modalities showed significant correlation ($R^2 = 0.954$, P = 0.0002; Fig. 2H, I).

### HIFU Simulation in Phantoms

To investigate the effect of PFCNE concentration on HIFU treatment, egg white-based phantoms with different PFCNE concentrations were insonated using different powers of focused ultrasound with constant mode (continuous wave) and duration (15 s). Under the same HIFU conditions, phantoms with 0.6 mg/mL PFCNE showed the largest lesion volumes, with the exception of the 2.51 MPa HIFU condition (Fig. 3). Higher concentrations of PFCNEs produced smaller lesion volumes that were comparable to lesions generated in phantoms without PFCNEs.
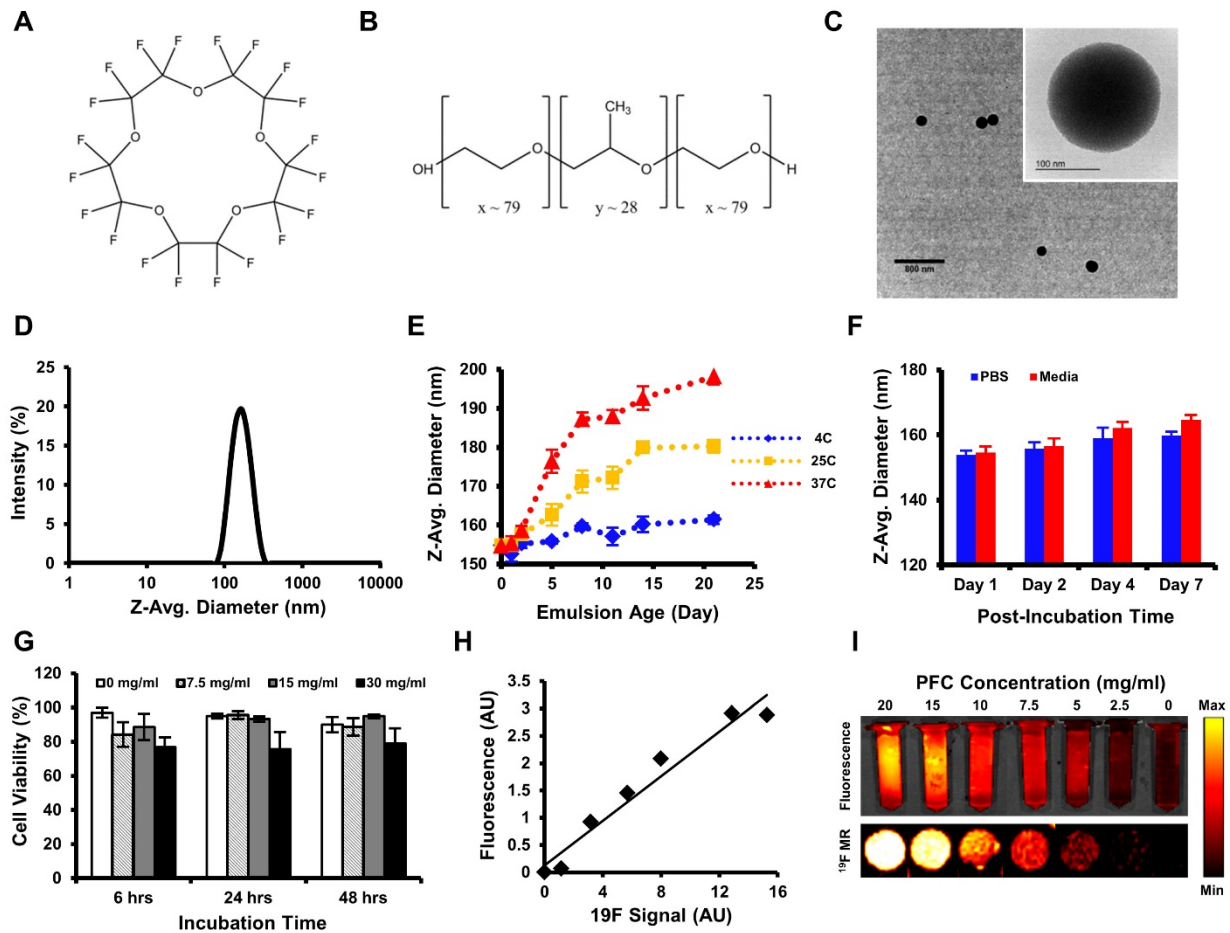
**Figure 2.** *In vitro* characterization of perfluorocarbon nanoemulsions (PFCNEs). Chemical structures of (A) perfluoro-15-crown-5-ether and (B) Lutrol F68. (C) Transmission electron microscopy image of PFCNE (scale bar = 800 nm for low magnification and 100 nm for the inset). (D) Size distribution of PFCNEs immediately after formulation. (E) Long term tracking of PFCNE size while subjected to 3 different temperatures for up to 3 weeks. (F) Serum stability of PFCNE incubated at 37°C. (G) HCT116 cell viability after PFCNE treatment. (H) Correlation of fluorescence signal and ¹⁹F MR signal intensity of PFCNE. (I) Fluorescence image (top row) and ¹⁹F MR images (bottom row) of reference tubes with various PFCNE concentrations.
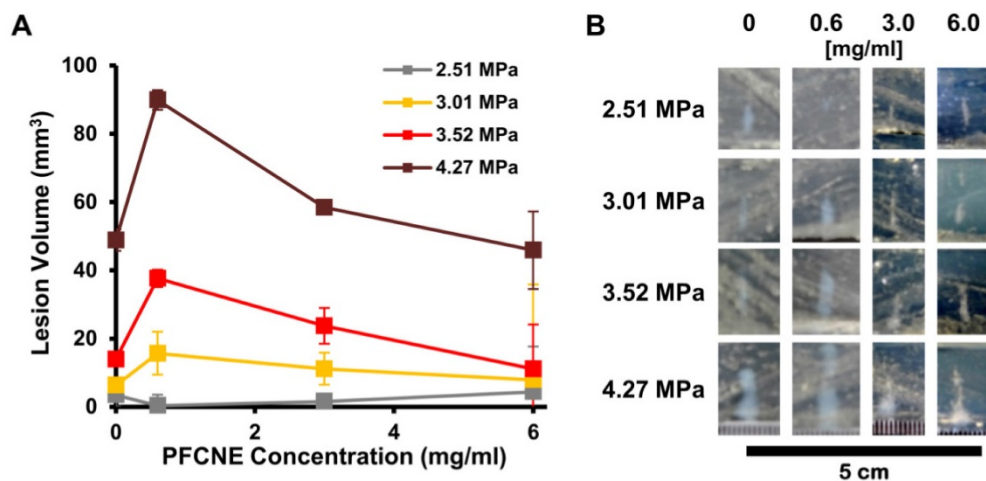


**Figure 3.** *Ex vivo* simulation of high intensity focused ultrasound (HIFU) ablation. (A) Volumes of lesions formed by HIFU of different peak-negative pressures in tissue phantoms with various perfluorocarbon nanoemulsion (PFCNE) concentrations. (B) Photographs of lesions formed in the phantoms.
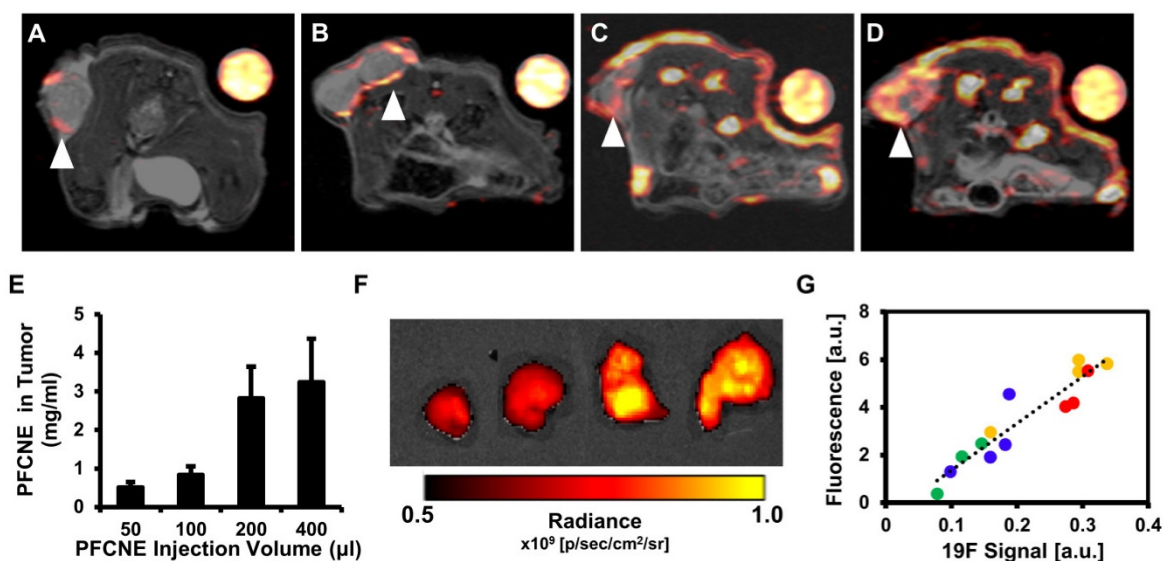
**Figure 4.** *In vivo* $^{19}$F magnetic resonance imaging (MRI) and signal quantification. (A-D) $^1$H/$^{19}$F merged images of mice injected with 50 μL (A), 100 μL (B), 200 μL (C), and 400 μL (D) of perfluorocarbon nanoemulsion (PFCNE). PFCNE is mostly accumulated in the tumor rim (arrowhead). (E) Quantification of PFCNE accumulated in tumor. A significant increase in accumulation is observed when the dosage increases from 100 μL to 200 μL. (F) Fluorescence images of excised tumors from mice injected with 50, 100, 200, and 400 μL of PFCNE (left to right). (G) Correlation of fluorescence intensity and $^{19}$F MR signal intensity from excised tumors (green: 50 μL; blue: 100 μL; yellow: 200 μL; red: 400 μL).

## In Vivo MR Tracking of PFCNE

Before HIFU treatment, $^{19}$F MR images of mice with a reference tube were acquired to visualize the distribution of PFCNEs and quantify them in tumors. With increasing dosage, higher accumulation of PFCNEs was detected in the tumor rims, as expected by the size of PFCNEs as well as the EPR effect (Fig. 4A–D). In the PFC400+ group, $^{19}$F MR signal was also detected in the tumor core, which may be attributed to the migration of splenic macrophages that had engulfed the injected PFCNEs. The amount of PFCNE in a tumor was quantified based on the signal intensity of the reference tube. Upon injection of 50, 100, 200, or 400 μL volumes, intra-tumoral PFCNE concentrations were found to be 0.52 ± 0.34, 0.84 ± 0.56, 2.83 ± 3.54, and 3.25 ± 2.74 mg/mL, respectively (Fig. 4E). To verify these quantities, tumors were excised and fluorescence images were acquired (Fig. 4F). Significant correlation between fluorescence and $^{19}$F MR signal intensity was observed ($R^2$ = 0.874, $P <$ 0.0001).

## Lesion Delineation by IVIM Mapping

HIFU-ablated lesions were clearly delineated by elevated levels of diffusion coefficients (Fig. 5A). In all HIFU-treated groups, $D_t$ values in lesions rapidly increased after HIFU treatment from ~5 × 10$^{-4}$ mm$^2$/s to ~1 × 10$^{-3}$ mm$^2$/s and remained stable up to day 14 (Fig. 5B). The sustained increase of $D_t$ may be explained by chronic inflammation accompanied by edema. The PFC200+ group showed the largest increase throughout the experimental period, but was not significantly higher than the other HIFU-treated groups. In the PFC200+ group, lesion volume decreased on day 1, but rapidly increased by day 7 (24.3±14.8 mm$^3$) while the volumes of the other groups remained constant or increased slowly (Fig. 5C). By day 7, the average lesion volume of the PFC200+ group was significantly higher than that of the PFC- group (Fig. 5C). Comparison of PFCNE amounts and $D_t$ in lesions showed a correlation in that increasing the PFCNE concentration up to 3 mg/mL caused a greater increase in $D_t$; however, the increase in $D_t$ was smaller with PFCNE concentrations above 3 mg/mL (Fig. 5D). Correlation of lesion volume and PFCNE concentration in a tumor also suggests that approximately 3 mg/mL of PFCNE in a tumor generates the largest lesion volume (Fig. 5E).

## BLI

Immediately after HIFU insonation, a significant decrease of the BLI signal was observed from all HIFU-treated groups (Fig. 6A). In particular, the PFC200+ group showed the most significant decrease in the BLI signal, which was reduced by 76.4 ± 8.88% (Fig. 6B). In all HIFU-treated groups, the BLI signal dropped on day 1 and gradually recovered to the original level before HIFU treatment by day 14 (Fig. 6B, C). Similar to the results observed with IVIM, increasing PFCNE concentration up to 2–3 mg/mL generated a larger BLI signal reduction. PFCNE concentrations above 3 mg/mL produced a smaller BLI signal reduction (Fig. 6D).
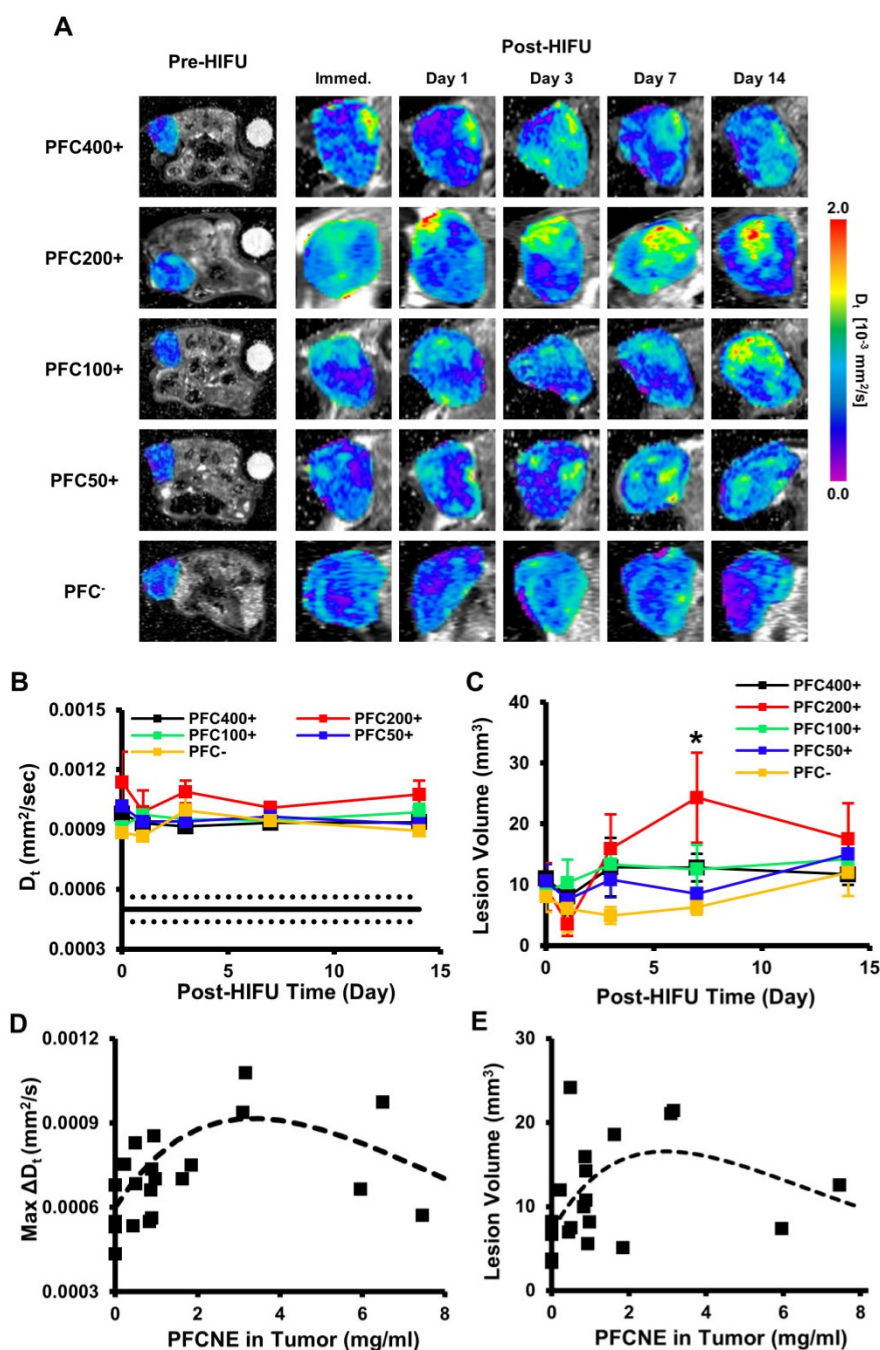
**Figure 5.** Intra-voxel incoherent motion (IVIM) analysis of ablated lesions. (A) Longitudinal $D_t$ maps of mice before and after high intensity focused ultrasound (HIFU) treatment. Ablated lesions are marked by increased $D_t$ values. (B) $D_t$ values of lesions over time beginning immediately after HIFU treatment (day 0). The black line indicates the median $D_t$ of tumors before HIFU treatment, and the dashed lines indicate the standard deviation. (C) Lesion volume changes over time beginning immediately after HIFU treatment (day 0) as a function of perfluorocarbon nanoemulsion (PFCNE) volume (*$P < 0.05$ vs. PFC-). (D) Correlation of the maximum lesion $D_t$ increase and tumor PFCNE concentration. The dashed line indicates the trend of the data. (E) Correlation of lesion volume and PFCNE concentration in tumor, measured on day 7. The dashed line indicates the trend of the data.

## Histological Analysis

Ablated lesions were clearly visible in H&E stained sections of all groups treated with HIFU (Fig. 7). Ballooning degeneration was commonly observed in the peripheral zones of lesions from all groups, forming a borderline between the lesion and non-ablated viable zone. The central zone of the lesion was highly variable among the groups. Red coloration by hemorrhage was observed in the PFC- group, and the PFC50+ group showed small necrotic regions scattered in the central zone. The PFC100+ group showed dilated blood vessels due to the heat generated by HIFU treatment. The PFC200+ group showed the most severe effect with complete necrosis and few cellular remnants. The central zones of lesions in the PFC400+ group did not show marked differences from the viable regions.
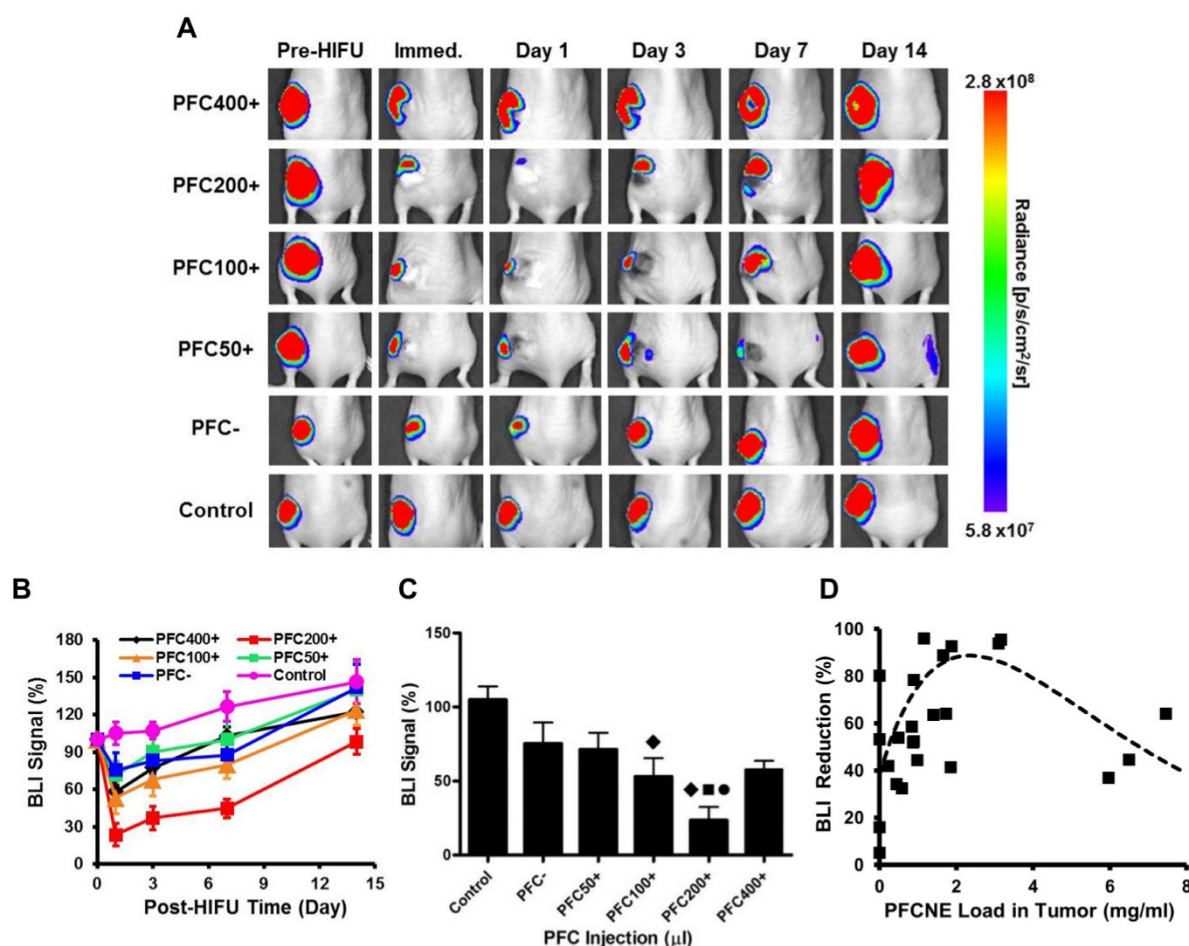
**Figure 6.** Longitudinal bioluminescence imaging (BLI). (A) BLI of mice before and after high intensity focused ultrasound (HIFU) treatment. (B) BLI signal intensity measurements after HIFU treatment. (C) Comparison of BLI signal intensities of animal groups measured immediately after HIFU treatment (◆: $P < 0.05$ vs. control; ●: $P < 0.05$ vs. PFC-; ■: $P < 0.05$ vs. PFC50+). (D) Correlation of BLI signal reduction and PFCNE concentration in a tumor. The dashed line indicates the trend of the data.

## Discussion

In this study, we demonstrated the feasibility of combining HIFU treatment with $^{19}$F MRI for precise and efficient ablation of tumors through quantitative tracking of PFCNEs. PFCNEs maintained appropriate size and stability with minimum cytotoxicity while enhancing thermal ablation in a tissue phantom. The accumulation of PFCNE in the tumor rim was clearly visible and quantifiable through $^{19}$F MRI. The effects of PFCNE on tumor ablation were non-invasively determined using IVIM analysis and BLI, and were subsequently confirmed by histological examination.

PFCNEs are widely studied as enhancers of HIFU tumor ablation. Yet, the correlation between their amounts in tumors and the efficiency of HIFU ablation remains undetermined. To estimate the effects of PFCNE amounts in HIFU tumor ablation, we used egg white phantoms incorporating various concentrations of PFCNE. Through applying HIFU with different acoustic pressures, we established a relationship between PFCNE concentration and lesion volume made in an egg white phantom (Fig. 3A); the largest lesion was produced with 0.6 mg/mL of PFCNE, concentrations above which lesion sizes decreased. Similar trends were observed *in vivo*; in both IVIM (Fig. 5C, E) and BLI (Fig. 6D) settings, peak ablation was achieved at 2–3 mg/mL of PFCNE. The decreased ablation at higher concentrations of PFCNE may be due to PFCNE coalescence, as the frequency of HIFU at which the PFCNE initiates cavitation activity is highly dependent on its size [29]. Further investigation is required to clarify the underlying mechanism.

Not only can the amount of PFCNE in a tumor be confirmed by $^{19}$F MRI and correlated with therapeutic efficacy of HIFU, but the distribution of PFCNE in a tumor can be determined as well. We administered PFCNE through intravenous injection to mimic the drug administration method used in the clinic. This method of delivery caused most PFCNEs to accumulate only in the periphery of a tumor;

therefore, direct intra-tumoral injection may be a more favorable method for achieving various patterns of intra-tumoral distribution of PFCNEs. Although direct injection is a clinically limited approach, it may facilitate controlling the distribution of PFCNE as well as observing the effect of PFCNE cavitation more clearly at a lower dosage.

IVIM served as a proof-of-principle that MR parametric analysis can be simultaneously performed with $^{19}$F MRI [30]. Although no significant difference was observed among HIFU-insonated groups in terms of $D_t$ value increase in lesions (Fig. 5B), the volumes of lesions in the PFC200+ group dramatically increased up to day 7, and were significantly larger than those observed in the PFC- group (Fig. 5C). The

lesion volume development over time may be associated with inflammatory edema. While IVIM provides information on changes in water diffusion due to cellular and nuclear membrane disruption, other physiological responses to HIFU ablation, such as protein denaturation and halted metabolism, can also be assessed through alternative parametric MR analyses (amide proton transfer imaging, MR spectroscopy, etc.) that are also compatible with $^{19}$F MRI. [31, 32]. Performing these parametric analyses along with $^{19}$F MRI will provide a thorough understanding of the effects of PFCNE in HIFU treatment.
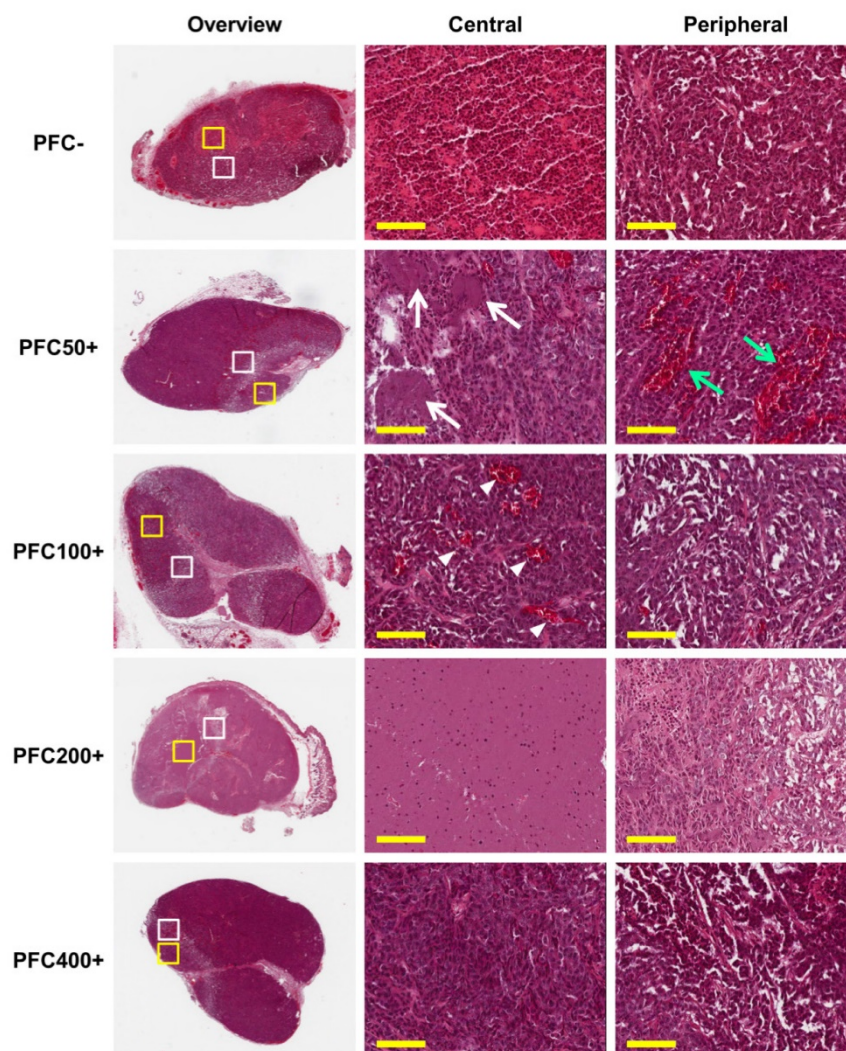


**Figure 7.** Histology of tumors after high intensity focused ultrasound (HIFU) treatment. HIFU-ablated regions are clearly visible in low magnification (10×) overview (dashed lines). Higher magnification images (200×, scale bar: 100 μm) were acquired in the central zone (yellow box) and peripheral zone (white box) of ablated lesions. All groups show ballooning degeneration in the peripheral zone of the ablated lesions; the PFC50+ group additionally shows dilated blood vessels (green arrows). Different degrees of necrosis and histological features were observed in the central zone depending on the amount of PFCNE injection (PFC-: hemorrhage; PFC50+: scattered necrotic zones [white arrows]; PFC100+: dilated blood vessels [white arrowheads]; PFC200+: complete necrosis with few cell remnants; PFC400+: no significant changes observed).

BLI showed a significant decrease of tumor viability immediately after HIFU treatment (Fig. 6). This decrease was observed on day 1, although recovery was observed beginning on day 3 and was complete by day 14. This indicates that the tumors were not completely ablated and were able to recur. While the cause of relapse was not investigated at a molecular level, immunohistochemistry and/or flow cytometry can be performed in the future to evaluate whether candidate molecules such as hypoxia-inducible factor 1-alpha and M2-phenotype tumor-associated macrophages are involved in tumor cell changes after HIFU treatment [33, 34]. For now, we treated each mouse with a single shot of HIFU to clearly distinguish an ablated lesion from any viable tumor portions. We postulate that repeated treatment with HIFU may completely ablate tumors and suppress their growth, leading to clearer differentiation of the effect of PFCNEs on HIFU ablation as determined by both IVIM mapping and BLI.

To increase the therapeutic efficiency and suppress tumor recurrence, anti-cancer drugs can be loaded onto PFCNEs so that tumors are ablated not only by the thermal dose from PFCNE cavitation but also by drugs released from these same PFCNEs. In many cases, sensitive tissues surrounding a tumor hinder complete ablation and leave viable tumor margins. It was previously shown that concurrent therapy with HIFU plus anti-cancer drugs suppresses tumor growth more effectively by destroying the tumor margins; this cannot be accomplished by HIFU alone [35]. Therefore, $^{19}$F MRI ought to play a significant role in such synergistic therapies, as the amount of drug delivered to a tumor can be quantified if the drug loading efficiency is calculated.

We used PCE for formulating PFCNEs, although other PFCs with lower boiling points such as perfluoropentane (PFP) and perfluorohexane are more widely used for HIFU ablation [36]. We chose PCE because it has 20 equivalent $^{19}$F atoms that generate a strong single nuclear magnetic resonance peak without any chemical shifts upon imaging. The echogenicity of PCE is also comparable to that of PFP; hence, nanoemulsions formulated with PCE also significantly increase the thermal dose [25]. Still, it may be more advantageous in terms of therapeutic efficiency to use low boiling point-PFCs, and the feasibility of imaging such PFCs with $^{19}$F MRI should therefore be tested.

Up to 400 µL of PFCNE was injected into mice to achieve a high intra-tumoral concentration. While similar or even larger quantities of PFCNE were injected in previous studies to ensure MR visibility, such doses may be too large and might cause spleen engorgement and leakage into the small intestine through the bile duct [37-39]. Thus, the low sensitivity of $^{19}$F MRI must be overcome so that the injection dosage of PFCNE is kept to a minimum to alleviate safety issues. Improvements in $^{19}$F MR sensitivity are being made by using pulse sequences that generate a high signal-to-noise ratio (SNR). Such improvements include using balanced steady state free precession sequence [40] and adopting advanced image reconstruction techniques, such as compressed sensing algorithms that were shown to accelerate $^{19}$F MR scanning time 8-fold without compromising the SNR and spatial resolution [41]. Considering these improvements and a recent clinical trial involving cell therapy [42], $^{19}$F MRI is highly expected to enter clinical trials for guiding precise HIFU tumor ablation in the future.

## Conclusion

In this study, we showed that $^{19}$F MRI is a useful platform for guiding HIFU ablation of tumors by quantitatively tracking PFCNE accumulation. PFCNE accumulation in the tumor periphery was clearly visible and quantifiable, and was confirmed by fluorescence imaging. IVIM analysis was performed not only to assess therapeutic outcomes but also to demonstrate the feasibility of multi-parametric analysis along with $^{19}$F MR tracking of PFCNE delivery. Increased water diffusion was observed in the ablated lesions, indicating cellular and nuclear membrane disruptions as well as inflammatory edema. BLI was also performed to measure tumor viability after HIFU treatment. Both IVIM analysis and BLI showed that 2–3 mg/mL of PFCNE in a tumor produces optimal ablation, with a similar trend observed in phantom experiments. Going forward, $^{19}$F MRI will be a valuable tool for non-invasively optimizing the use of PFCNE in HIFU ablation, enabling more precise and robust HIFU treatment in future.

## Abbreviations

$^{19}$F: fluorine-19; ANOVA: analysis of variance; BLI: bioluminescence imaging; DWI: diffusion-weighted image; EPR: enhanced permeation and retention; HIFU: high intensity focused ultrasound; H&E: hematoxylin and eosin; IVIM: intra-voxel incoherent motion; MB: microbubble; MRI: magnetic resonance imaging; NA: number of average; PCE: perfluoro-15-crown-5-ether; PDI: polydispersity index; PFC: perfluorocarbon; PFCNE: perfluorocarbon nanoemulsion; PFP: perfluoropentane; RARE: rapid acquisition with relaxation enhancement; ROI: region of interest; SNR: signal-to-noise ratio; ST: slice thickness; TE: echo time;

TEMED: tetramethylethylenediamine; TR: repetition time; US: ultrasonography.

## Ethics Committee Approval

This study was reviewed and approved by the Institutional Animal Care and Use Committee (IACUC) of the National Cancer Center Research Institute. The Institute is an Association for Assessment and Accreditation of Laboratory Animal Care International-accredited facility that abides by the Institute of Laboratory Animal Resources guide.

## Competing Interests

The authors have declared that no competing interest exists.

## References

1. [Internet] Focused Ultrasound Foundation: Charlottesville, VA, USA. State of the technology. http://www.fusfoundation.org/the-technology/state-of-the-technology
2. Lukka H, Waldron T, Chin J, et al. High-intensity focused ultrasound for prostate cancer: a systematic review. Clin Oncol. 2011; 23: 117-27.
3. Ringold S. FDA approves ultrasound fibroid therapy. JAMA. 2004; 292: 2826.
4. Tempany CM, McDannold NJ, Hynynen K, et al. Focused ultrasound surgery in oncology: overview and principles. Radiology. 2011; 259: 39-56.
5. Gedroyc WM, Anstee A. MR-guided focused ultrasound. Expert Rev Med Devices. 2007; 4: 539-47.
6. Moyer L, Timbie K, Sheeran P, et al. Direct nanodroplet and microbubble comparison for high intensity focused ultrasound ablation enhancement and safety. J Ther Ultrasound. 2015; 3 (Suppl 1): O67.
7. Moyer LC, Timbie KF, Sheeran PS, et al. High-intensity focused ultrasound ablation enhancement in vivo via phase-shift nanodroplets compared to microbubbles. J Ther Ultrasound. 2015; 3: 7.
8. Kopechek JA, Park EJ, Zhang YZ, et al. Cavitation-enhanced MR-guided focused ultrasound ablation of rabbit tumors in vivo using phase shift nanoemulsions. Phys Med Biol. 2014; 59: 3465-81.
9. Zhang N, Cai X, Gao W, et al. A multifunctional theranostic nanoagent for dual-mode image-guided HIFU/chemo-synergistic cancer therapy. Theranostics. 2016; 6: 404-17.
10. Ma M, Xu H, Chen H, et al. A drug–perfluorocarbon nanoemulsion with an ultrathin silica coating for the synergistic effect of chemotherapy and ablation by high-intensity focused ultrasound. Adv Mater. 2014; 26: 7378-85.
11. Jo SD, Ku SH, Won Y, et al. Targeted Nanotheranostics for Future Personalized Medicine: Recent Progress in Cancer Therapy. Theranostics. 2016; 6: 1362-1377.
12. Miller MA, Gadde S, Pfirschke C, et al. Predicting therapeutic nanomedicine efficacy using a companion magnetic resonance imaging nanoparticle. Sci Transl Med. 2015; 7: 314ra183.
13. Song S, Guo H, Jiang Z, et al. Self-assembled $Fe_3O_4$/polymer hybrid microbubble with MRI/ultrasound dual-imaging enhancement. Langmuir. 2014; 30: 10557-61.
14. Chen Y, Chen H, Sun Y, et al. Multifunctional mesoporous composite nanocapsules for highly efficient MRI-guided high-intensity focused ultrasound cancer surgery. Angew Chem Int Ed Engl. 2011; 50: 12505-9.
15. Viglianti BL, Ponce AM, Michelich CR, et al. Chemodosimetry of in vivo tumor liposomal drug concentration using MRI. Magn Reson Med. 2006; 56: 1011-8.
16. Ahrens ET, Flores R, Xu H, et al. In vivo imaging platform for tracking immunotherapeutic cells. Nat Biotechnol. 2005; 23: 983-7.
17. Flögel U, Ding Z, Hardung H, et al. In vivo monitoring of inflammation after cardiac and cerebral ischemia by fluorine magnetic resonance imaging. Circulation. 2008; 118: 140-8.
18. Partlow KC, Chen J, Brant JA, et al. 19F magnetic resonance imaging for stem/progenitor cell tracking with multiple unique perfluorocarbon nanobeacons. FASEB J. 2007;21: 1647-1654.
19. Diou O, Tsapis N, Giraudeau C, et al. Long-circulating perfluorooctyl bromide nanocapsules for tumor imaging by 19F MRI. Biomaterials. 2012;33: 5593-5602.
20. Bulte JW. Hot spot MRI emerges from the background. Nat Biotechnol. 2005; 23: 945-6.
21. Wang YG, Kim H, Mun S, et al. Indocyanine green-loaded perfluorocarbon nanoemulsions for bimodal 19 F-magnetic resonance/nearinfrared fluorescence imaging and subsequent phototherapy. Quant Imaging Med Surg. 2013; 3: 132-40.
22. Ahrens ET, Young WB, Xu H, et al. Rapid quantification of inflammation in tissue samples using perfluorocarbon emulsion and fluorine-19 nuclear magnetic resonance. Biotechniques. 2011; 50: 229-34.
23. Takegami K, Kaneko Y, Watanabe T, et al. Polyacrylamide gel containing egg white as new model for irradiation experiments using focused ultrasound. Ultrasound Med Biol. 2004; 30: 1419-22.
24. Balducci A, Wen Y, Zhang Y, et al. A novel prove for the non-invasive detection of tumor-associated inflammation. Oncoimmunology. 2013;2: e23034.
25. Rapoport N, Nam K-H, Gupta R, et al. Ultrasound-mediated tumor imaging and nanotherapy using drug loaded, block copolymer stabilized perfluorocarbon nanoemulsions. J Contr Rel. 2011;153: 4-15.
26. Srinivas M, Morel PA, Ernst LA, et al. Fluorine-19 MRI for visualization and quantification of cell migration in a diabetes model. Magn Reson Med. 2007; 58: 725-34.
27. Le Bihan D, Breton E, Lallemand D, et al. MR imaging of intravoxel incoherent motions: application to diffusion and perfusion in neurologic disorders. Radiology. 1986; 161: 401-7.
28. Kim Y, Ko K, Kim D, et al. Intravoxel incoherent motion diffusion-weighted MR imaging of breast cancer: association with histopathological features and subtypes. Br J Radiol. 2016; 89: 20160140.
29. Humphrey VF. Ultrasound and matter—Physical interactions. Prog Biophys Mol Biol. 2007; 93: 195-211.
30. Bible E, Dell'Acqua F, Solanky B, et al. Non-invasive imaging of transplanted human neural stem cells and ECM scaffold remodeling in the stroke-damaged rat brain by (19)F-and diffusion-MRI. Biomaterials. 2012; 33: 2858-71.
31. Lam MK, Oerlemans C, Froeling M, et al. DCE-MRI and IVIM-MRI of rabbit Vx2 tumors treated with MR-HIFU-induced mild hyperthermia. J Ther Ultrasound. 2016; 4: 9.
32. Hectors SJCG, Jacobs I, Moonen CT, et al. MRI methods for the evaluation of high intensity focused ultrasound tumor treatment: current status and future needs. Magn Reson Med. 2016; 75: 302-17.
33. Semenza GL. Hypoxia, clonal selection, and the role of HIF-1 in tumor progression. Crit Rev Biochem Mol Biol. 2000;35:71-103.
34. Sica A, Bronte V. Altered macrophage differentiation and immune dysfunction in tumor development. J Clin Invest. 2007;117:1155-1166.
35. Wong AW, Fite BZ, Liu Y, et al. Ultrasound ablation enhances drug accumulation and survival in mammary carcinoma models. J Clin Invest. 2016;126: 99-111.
36. Matsunaga TO, Sheeran PS, Luois S, et al. Phase-change nanoparticles using highly volatile perfluorocarbons: toward a platform for extravascular ultrasound imaging. Theranostics. 2012; 2: 1185-1198.
37. Shi Y, Oeh J, Eastham-Anderson J, et al. Mapping in vivo tumor oxygenation within viable tumor by 19F-MRI and multispectral analysis. Neoplasia. 2013;15: 1241-1250.
38. van Heeswijk RB, Pellegrin M, Flögel U, et al. Fluorine MR imaging of inflammation in atherosclerotic plaque in vivo. Radiology. 2014;275: 421-429.
39. Bulte JWM, Schmieder AH, Keupp J, et al. MR cholangiography demonstrates unsuspected rapid biliary clearance of nanoparticles in rodents: implications for clinical translation. Nanomedicine. 2014;10: 1385-1388.
40. Ribot EJ, Gaudet JM, Chen Y, et al. In vivo MR detection of fluorine-labeled human MSC using the bSSFP sequence. Int J Nanomed. 2014; 9: 1731-9.
41. Zhong J, Mills PH, Hitchens TK, et al. Accelerated fluorine-19 MRI cell tracking using compressed sensing. Magn Reson Med. 2013; 69: 1683-90.
42. Ahrens ET, Helfer BM, O'Hanlon CF, et al. Clinical cell therapy imaging using a perfluorocarbon tracer and fluorine-19 MRI. Magn Reson Med. 2014; 72: 1696-701.